Critical Role of Pressure for Chemo-Mechanical Induced Stability of Sodium Metal Battery Anodes

Weimin Jiao¹, Murtaza Zohair¹, Janna Eaves-Rathert³, Jayanth Ramaswami Ramamurthy¹, Rebecca Mort², Jacob Wheaton², Shan Jiang², Steve W. Martin² and Cary L. Pint*, ¹

¹Department of Mechanical Engineering, Iowa State University, Ames, Iowa 50011, United States. ²Department of Materials Science and Engineering, Iowa State University, Ames, Iowa 50011, United States. ³Department of Mechanical Engineering, Vanderbilt University, Nashville, Tennessee 37235, United States

AUTHOR INFORMATION

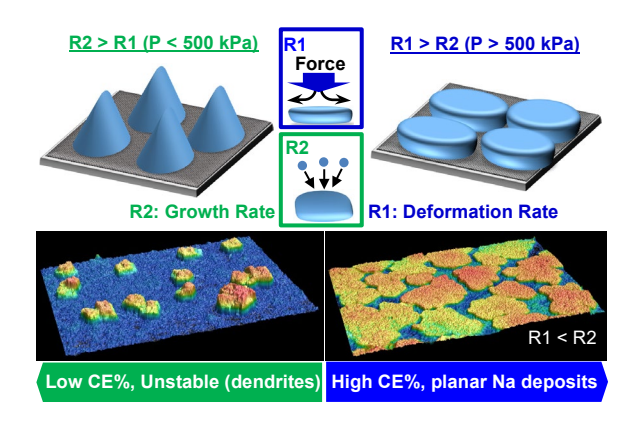
Corresponding Author

* carypint@iastate.edu

ABSTRACT:

In this work we demonstrate that cell pressure controls the morphology and stability of electroplated sodium metal deposits onto carbon black nucleation layers in ether-based electrolytes. At pressures below 500 kPa we observe the presence of three-dimensional sodium nuclei accompanied by low Coulombic efficiencies (less than 98%). Conversely, at pressures between 500 – 1270 kPa we observe smooth, planar sodium deposits, high Coulombic efficiencies up to 99.9%, and stable electrochemical cycling. Through a series of tests conducted at elevated current densities and with/without rest stages, our findings elucidate the important competing timescales of (1) creep-induced morphology evolution of the sodium under pressure, and (2) the rate at which sodium is electrodeposited. This highlights how chemo-mechanical effects at pressure ranges relevant for battery packaging in coin and pouch cells are a key factors in the design and operation of sodium metal batteries.

TOC GRAPHIC



Sodium (Na) metal is one of the most promising anode options for high-energy-density and low-cost Na-based batteries. With a high theoretical specific capacity (1166 mAh g⁻¹), low standard electrode potential (-2.71 V versus standard hydrogen electrode),¹⁻³ and native electrochemical stability in common electrolytes, there have been a number of reports in recent years highlighting the broad promise of this system. Most notably is the anode-free battery architecture, where researchers have shown up to 400 Wh/kg active mass energy density,⁴ and recent reports under lean electrolyte conditions in pouch cell architectures have demonstrated 200 Wh/kg.⁵ However, other frameworks include room-temperature Na-S batteries⁶⁻⁸ with theoretical energy density of 1274 Wh kg⁻¹ and Na-O2 batteries⁹⁻¹¹ with theoretical energy density of 1605 Wh kg⁻¹. Each of these systems exist in different developmental stages, but all of which exhibit improved energy density over current Li-ion batteries¹ at lower cost due to a combined 1000 times higher earth abundance of Na versus Li and lower cost and lighter options for cathode materials and current collectors, respectively.¹²⁻¹⁴

Early studies, focused on Na metal anodes, followed inspiration from Li metal anodes, with the expectation being that these two alkali metals are similar in behavior. Early observations of Na electroplating in carbonate electrolytes demonstrated similar behavior to Li, with unstable nucleation and growth of Na deposits accompanied by low Coulombic efficiencies and dendrite formation. However, researchers demonstrated that the use of ether-based electrolytes, such as diglyme, resulted in smooth crystalline electroplated Na deposits combined with Coulombic efficiencies (CEs) exceeding 99.9%. This highlights a critical difference of sodium metal batteries over lithium-metal batteries due to the less negative reduction potential of sodium that has given promise to competitive Na battery approaches. In this regard, other differences between Na and Li exist, such as in mechanical and thermal properties, that have not been deeply

investigated. Specifically, in regard to mechanical properties, Na is softer at room temperature than Li in metal form with elastic modulus of 4.6 GPa for Na, and 7.82 for Li. 18, 19 Notably, the stress exponent for Na has been measured to be 5 versus 6.56 for Li, indicating that Na is far more susceptible to creep than Li. 18-20 As creep effects do not occur in Li metal until pressures much higher than that of commercial batteries, there exists limited understanding of how the chemo-mechanical effects in sodium metal impact a sodium metal battery differently than lithium in a lithium metal battery.

With this said, researchers have demonstrated that applying high external pressure is a significant and effective approach to modify the chemistry and stability of Li metal deposits. Yin *et al.* reported a 5% improved CE% during Li deposition in Li cells at 1.1 MPa pressure²¹ and Shen *et al.* ascribed such effects to modifications in Li morphology.²² In this regard, there has been limited research to understand the role of pressure in Na metal batteries and that has been limited to understanding how pressure modifies Na metal interfaces.^{23, 24} Therefore, given the lower modulus of sodium compared to lithium, which makes Na metal more sensitive to the pressure range of conventionally packaged pouch and coin cells, there is need to better understand the pressure-induced chemo-mechanical effects in sodium metal batteries.

In this report, we systematically study the role of pressure on the nucleation, growth, and electrochemical properties of sodium by combining imaging and electrochemical studies to understand the role of pressure on sodium metal batteries. Our findings demonstrate that not only is sodium nuclei formation and growth morphology highly correlated to pressure due to Na creep in the pressure range relevant to commercially packaged batteries (less than 1.3 MPa), but also that pressure induced morphology changes modify and improve the electrochemical stability of the sodium metal deposits. Our results explain this as a chemo-mechanical trade-off between

the rate of Na charge transfer and the creep rate of Na under pressure, leading to a direct mechanical-electrochemical picture of stability in sodium metal anodes.

Results and Discussion

A key motivation for this work originated from the observation that in an in-situ characterization cell without the external application of pressure, 3-D and/or dendritic morphologies of Na were observed during Na electroplating. Comparatively, coin cells packaged under standard pressures between 500-1000 kPa under similar current densities led to smooth, planar morphologies of electrodeposited Na. To investigate this unexpected result, we designed a closed pressure-electrochemical cell (supporting information, Figures S1 and S2) to controllably apply pressure to a sodium electrode assembly consisting of 1 M NaPF₆ in diglyme, Celgard separator, Al/Na electrode, and Al/carbon black nucleation layer (details included in supporting information). A schematic of the cell and confocal laser scanning microscopy (CLSM) images showing the widely different nucleation behavior of Na over 30 mins at current density 0.5 mA cm⁻² with (1) no external pressure and (2) a pressure of 911 kPa are shown in Figure 1. With no external pressure, the formation of nuclei that protrude from the surface in a 3D growth mode (Figure 1A and B) are observed. Under uniaxial pressure (Figure 1C) of 911 kPa on the electrode assembly, smoother and lateral growth was observed for Na nuclei (Figure 1D and E). This observation elucidates that pressure plays an important role in Na nuclei morphology in a battery.

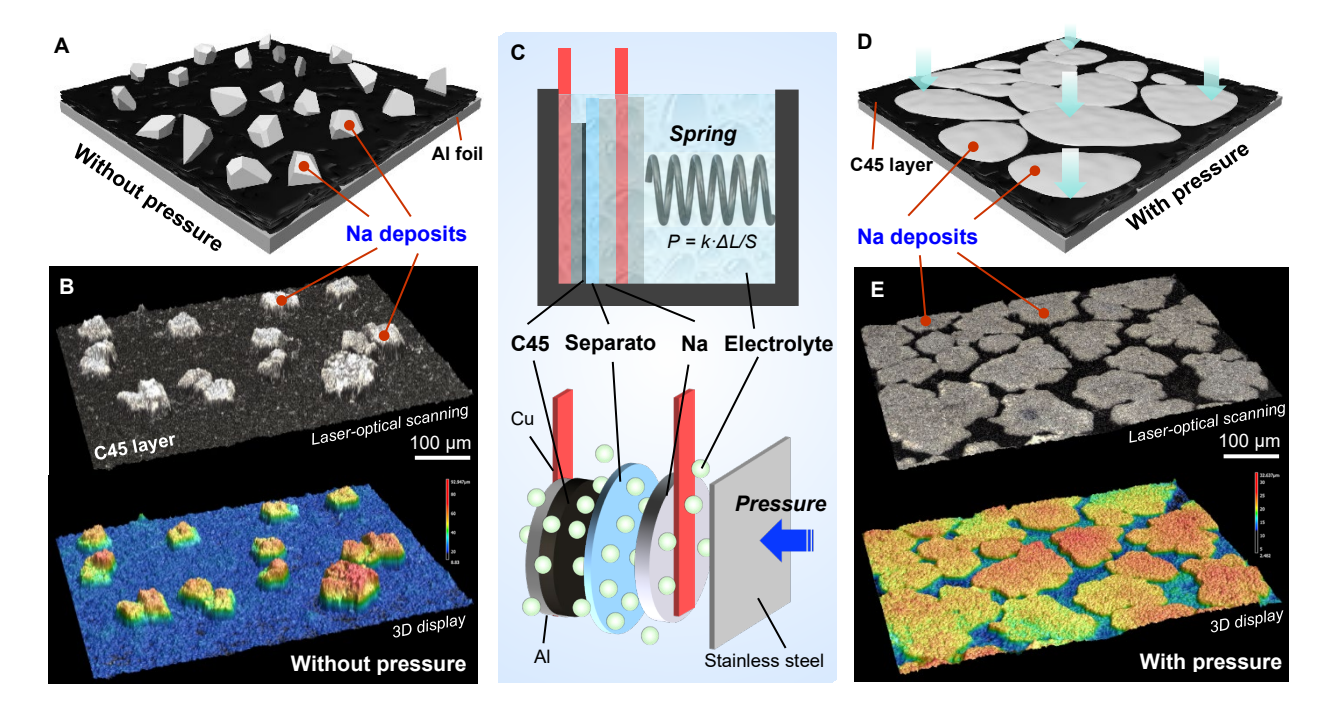


Figure 1. The impact of applied external pressure on Na electrodeposition. (A) Schematic illustration and (B) CLSM image of the Na deposits without pressure. (C) Schematic of the pressure experiment set-up and the assembling configuration of Na-thin C45 carbon black nucleation layer/Al current collector cell. (D) Schematic illustration and (E) CLSM image of the Na deposits without pressure.

To systematically study the effect of pressure on Na metal nucleation and growth during electrodeposition, we analyzed electrochemical and morphological behavior of Na electroplating under six different pressure conditions, 0, 22, 136, 500, 911, and 1272 kPa. Generally, as the pressure inside of a coin cell assembly is near ~ 1 MPa, this range of pressures gives detailed resolution of effects on electroplating between low pressures and those practical to battery packaging. To study the role of pressure on the cells, we carried out Galvanostatic tests (Figure S3) at 0.5 mA cm⁻² and subsequent imaging of the sodium morphology via confocal laser scanning microscopy and scanning electron microscopy. To benchmark pressure effects on the Na battery system, we assembled coin cells of the same electrode materials as used in our

pressure cell, and observed a high average CE% of 99.93% over a period of 1000 cycles (Figure S4), indicating competitive performance with leading state-of-the-art reports in recent literature. However, to understand and distinguish the role of pressure, especially in the early stages of formation, we carried out galvanostatic cycling at different pressures for 50 cycles, which leads to a slightly lower overall average CE% due to the influence of the first several cycles. Figure 2A shows the plating-stripping curves of the 2nd cycle for each pressure condition studied using slip plots to visualize the losses. Notably, the 2nd cycle loss decreased from 46.08% at 0 kPa to only 2.04% at 1272 kPa indicating improved stability. Figure 2B shows the CE% for each cycle and average CE% for each pressure over the period of 50 cycles studied indicating an evident correlation. The average CE% values at 0 kPa, 22 kPa, 136 kPa, and 500 kPa were 81.89%, 95.94%, 99.05% and 99.59%, respectively, over 50 cycles emphasizing that the largest sodium metal losses occurred in the first 50 cycles at the lowest pressures. At pressures greater than 500 kPa, there was only slight increases to the CE% over a 50 cycle duration.

Further, to better understand this influence of pressure, electrochemical impedance spectroscopy (EIS) was carried out. At the open-circuit voltage (OCV) prior to sodium electroplating (Figure S5), the charge-transfer resistance (Rct) is similar for all pressures except for the highest pressure (1272 kPa), where Rct is slightly lower. However, EIS analysis after the second Na plating cycle (Figure 2C) indicates much different characteristics, where the value of Rct significantly decreases based on the pressure applied to the cell. The cell at 0 kPa displays higher Rct (\sim 110 Ω cm²) than cells under pressure and there is little effect on the value of Rct after the pressure is increased beyond \sim 500 kPa (a range of 3.4 – 3.7 Ω cm²). These observations indicate the effect of pressure on performance does not occur in open circuit conditions before sodium is electroplated, but occur and evolve in tandem with sodium metal electrodeposition. To

better elucidate this, the voltage polarization under different applied pressures was studied (Figure 2D), which quantifies the difference between the equilibrium plating and stripping potentials for Na (Figure S6). Similar to pressure effects on the CE%, the average voltage hysteresis decreased when the pressure increased until near 500 kPa, with minimal changes at higher pressures.

Collectively, the electrochemical results in Figure 2 indicate that both charge loss and charge-transfer resistances are reduced when pressure is increased. Whereas pressure effects have been observed in Li metal cells, 21, 25, 26 these effects observed for Na metal cells here are notably at lower and more practical pressures (near 0.5 kPa) where damage to the separator does not influence transport. An alternative explanation for EIS results could be explained by improved pressure-induced wetting at the current collector – electrolyte interface. Such wetting effects, however, cannot explain the significant change in stability of the electrodeposited Na as evident in CE% results. Therefore, to better understand this observation and the mechanism driving these pressure-induced differences, we carried out studies of electrodeposited Na morphology using both confocal laser scanning microscopy (CLSM) (Figure 3) and scanning electron microscopy (SEM) (Figure 4).

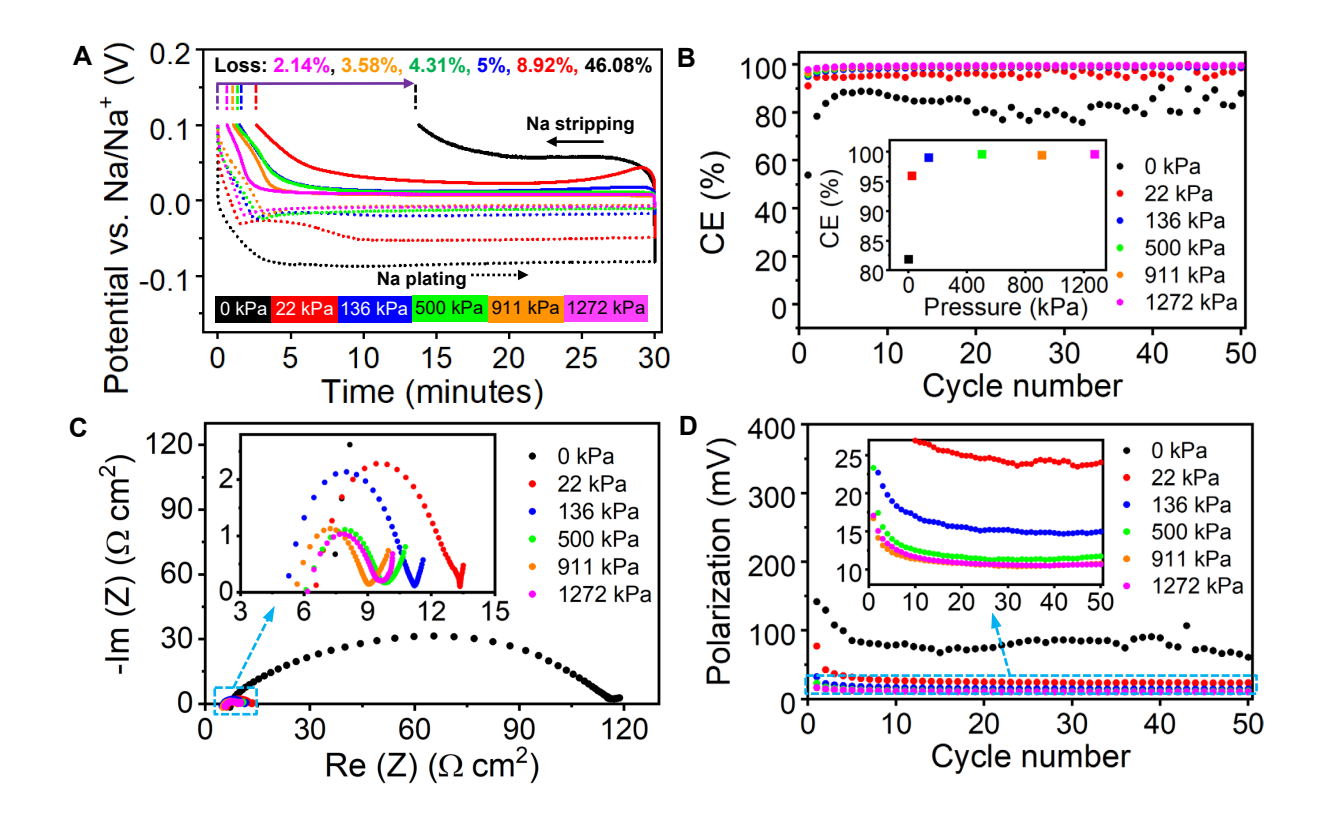


Figure 2. The electrochemical performances of the Na -C45 cell under various external pressures. (A) Slippage profiles for Na plating and stripping in the second cycle performed at 0.5 mA cm⁻² under different pressures. (B) Coulombic efficiency (CE) from 50 plating/stripping cycles and the average CE under different pressures performed at 0.5 mA cm⁻² with capacity of 0.25 mAh cm⁻². (C) Nyquist curves performed under different pressures after second cycle deposition. (D) Voltage polarization under various pressures.

To perform morphological characterization of Na deposits, we first utilized CLSM in an airtight optical cell (Figure S7) to study microscale morphology of Na deposits on C45 nucleation layers at different pressures (Figure 3A-F). CLSM is a non-contact analysis technique that provides micron-scale resolution in the x-y plane parallel to the current collector, and nanometer scale resolution in the z (height) plane. Notably, from pressures of 0 - 500 kPa, the morphology of Na deposits undergoes a drastic transition from 3D nuclei structures at low pressures to

smooth and heterogeneous planar deposits near and above 500 kPa. At pressures higher than 500 kPa, the overall morphology of the deposits did not significantly change, but the deposits were more interconnected at higher pressures. To quantify the role of pressure on the properties of sodium deposits, several representative CLSM images at different pressures were subjected to laser measurement in the CLSM and image processing methods (ImageJ²⁷) were used to identify geometrical characteristics including (1) average thickness of Na deposits (Figure 3G, by laser on CLSM), (2) average area of Na deposits (Figure 3H, by ImageJ), and (3) fractional area of Na on the current collector (Figure 3I, by ImageJ). In each case, results are presented in a statistical dot-plot representation to establish how each geometrical feature changes as a function of pressure. As shown in Figure 3G, the average Na deposit thickness at 0 kPa is ~42.2 µm (with significant height variation) which decreases to ~ 7.6 µm at 1272 kPa in a compact range of values. A similar observation is made in the average individual Na deposit area as the average deposit scales from ~5829 µm² to ~22242 µm² from 0 to 911 kPa (Figure 3H). Due to the interconnected nature of sodium deposits at 1272 kPa, the total coverage was also analyzed (Figure 3I), and shows the coverage fraction of Na improves from 14.9% at 0 kPa to 86.1% at 1272 kPa.

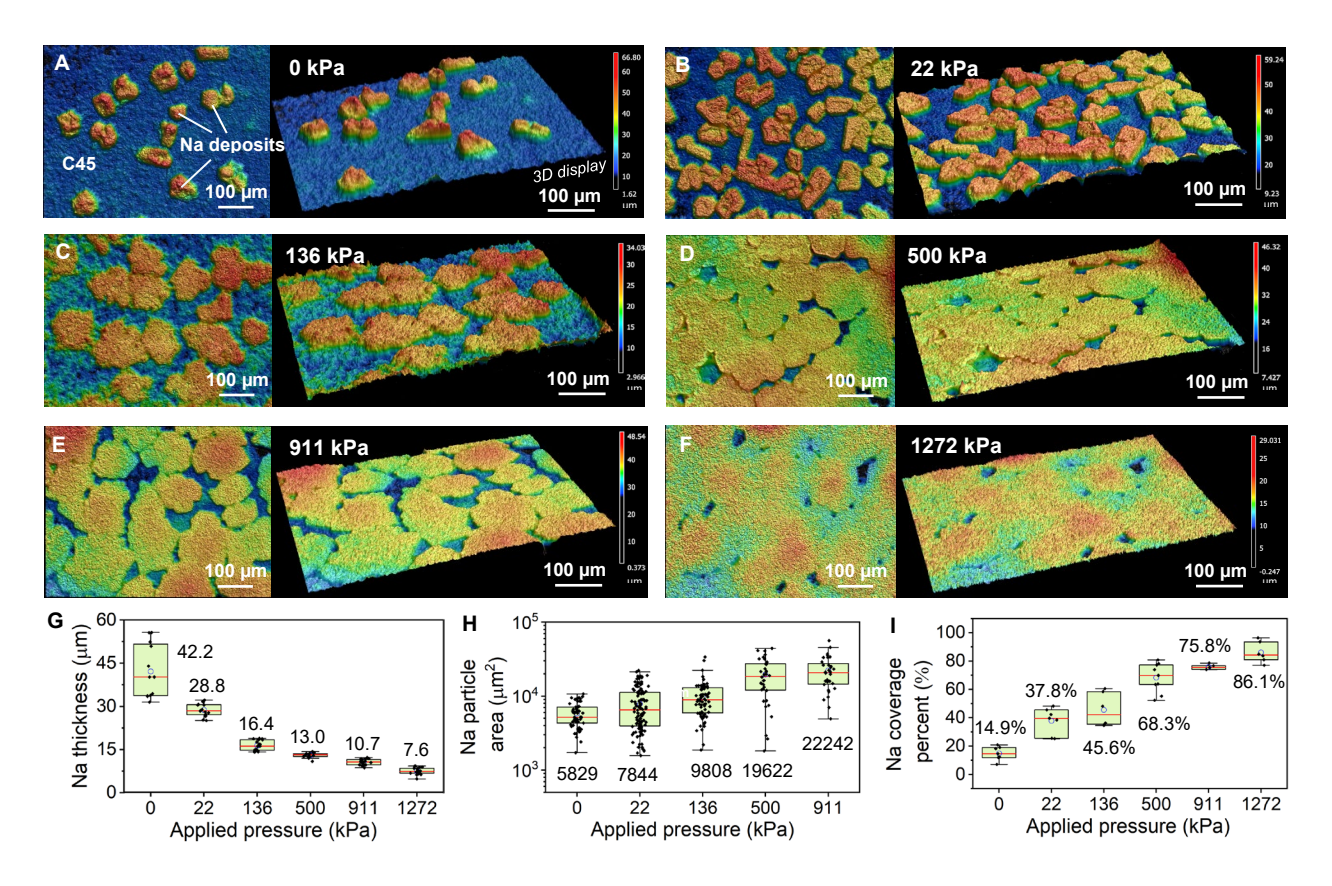


Figure 3. Growth pattern and physical feature of Na after second deposition under various pressures. (A-F) Top and 3D view of Na deposited under (A) 0 kPa, (B) 22 kPa, (C) 136 kPa, (D) 500 kPa, (E) 911 kPa and (F) 1272 kPa at 0.5 mA cm⁻² for 0.5 h. (G-I) The corresponding thickness (G), individual area (H) and area coverage fraction on C45 layer (I) of Na deposition under various pressures obtained from CSLM test.

While CLSM is a valuable tool to visualize the morphology changes of Na at different pressures, it does not enable the resolution to assess the microstructure of the sodium, such as the porosity. However, comparing the analysis of CLSM images to calculations of fully dense sodium at capacity of 0.25 mA cm⁻², the theoretical thickness of the sodium at 86% coverage should be 2.5 µm, which is lower than that observed in imaging. This suggests that microstructure and porosity in the sodium deposits could also be changing at different pressures. To evaluate this point, SEM analysis was carried out (Figure 4) using a sealed Ar transfer cell

that inhibits air exposure during transfer between the glove box and the SEM. At 0 kPa (Figure 4A), porosity in the Na deposits exist at both the microscale and nanoscale as is expected in 3D deposits. However, as the pressure is increased to and above 500 kPa, the pores in the Na deposits become smaller and are too small to resolve at pressures of 911 kPa and above. This supports that the effect of pressure on morphology is manifested both in microscale morphology (e.g. 2D versus 3D deposits) as well as the nanoscale porosity of the Na layers.

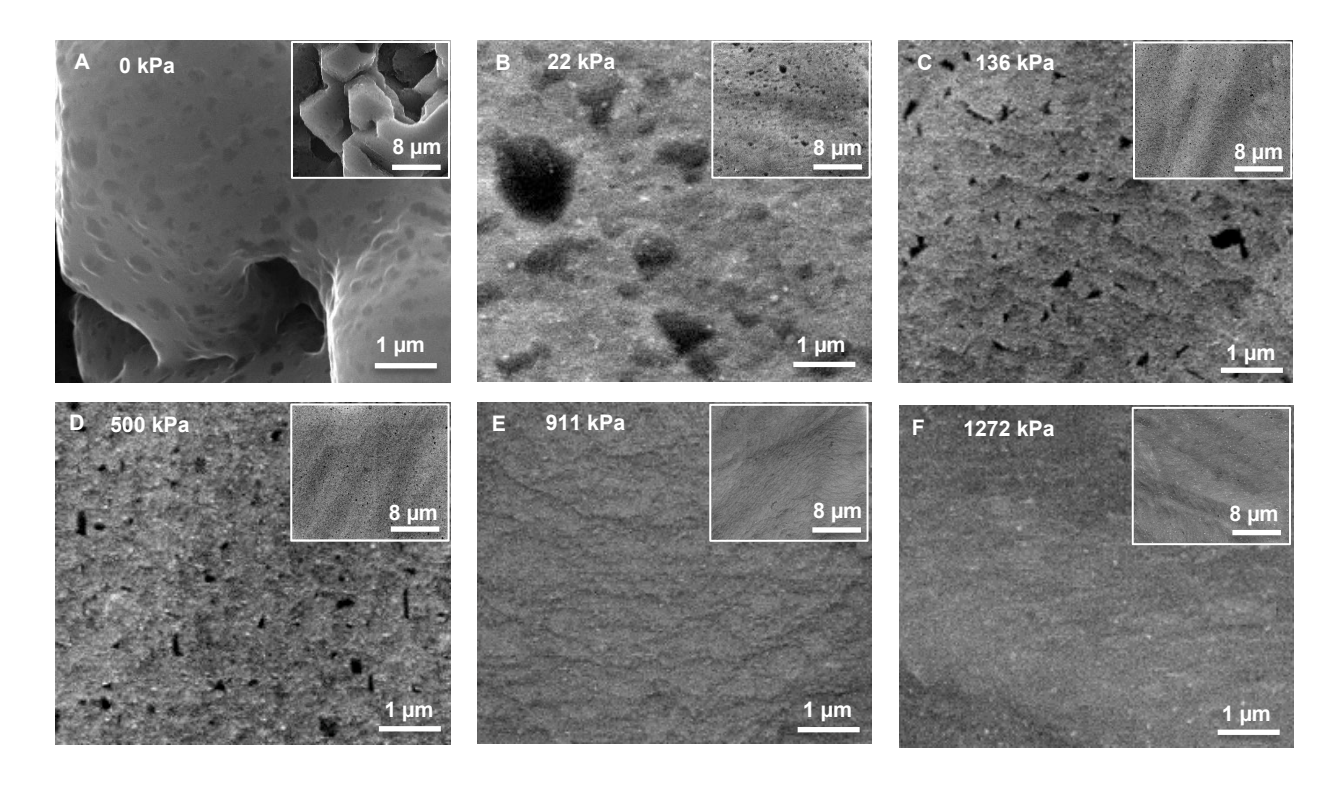


Figure 4. SEM images of Na deposition under various pressures after second plating at 0.5 mA cm⁻² to a capacity of 0.25 mAh cm⁻². (A-F) Surface morphology of Na deposited under (A) 0 kPa, (B) 22 kPa, (C) 136 kPa, (D) 500 kPa, (E) 911 kPa and (F) 1272 kPa. The insets in (A-F) show their respective minified SEM images.

In considering the results presented this far, it is clear that increasing pressure leads to thinner, more uniform, and less porous (more dense) Na deposits, especially at pressures near

and above 500 kPa (Figure 3, Figure 4). At pressures where 3D Na deposits are observed (< 500 kPa), the electrochemical features indicate poorer charge reversibility and greater interfacial resistances for charge transfer (Figure 2). This opens a key question as to whether the changes in Na morphology observed are static, or occur at nucleation, or are dynamic and continuously evolving through the electrochemical process. Prior modeling studies have shown that pressure can influence the static shape profile of 3D dendritic Li metal structures, ²² and dynamic effects such as creep are not feasible at pressures near and below 1 MPa for Li.23 However, the mechanical properties of Na are significantly different from that of Li – the stress exponent for Na is 5 versus 6.56 for Li, indicating a much greater influence of creep with Na metal. 18-20 Furthermore, the effective hardness of Na is 15 MPa versus 48 MPa for Li.^{23, 28} Recent results have shown that at solid-solid interfaces at 1 MPa pressures, creep effects can modify the Na metal interface properties.²³ To evaluate the static versus dynamic response of Na deposits to pressure (Figure 5), we carried out a study in a coin cell configuration (~ 1 MPa, Figure S8) where 10x higher plating/stripping current of 5 mA cm⁻² is used since this represents the current range at coin cell pressures at which shorting effects occur under normal cycling (Figure S9 and Figure 5F).

To evaluate the dynamic behavior of the electroplated sodium under pressure, we compared electrochemical and morphological characteristics of sodium deposits after plating both with and without a 2 hour rest stage (Figure 5A and 5B). In this experiment, the rest step of 2h is chosen as it allows the electrodeposited Na to reach an equilibrium state under pressure with a rationale analogous to that of rest steps in Galvanostatic Intermittent Titration Technique (GITT) experiments. As shown in Figure 5, and illustrated in Figure 5C, the morphology and electrochemical characteristics of the Na deposits are highly susceptible to dynamic changes and

morphology evolution during this rest step. CLSM images of Na deposits without rest and with rest under pressure (Figure 5D, 5E) show a more interconnected, thinner (by over 25%), and planar film after undergoing a 2h rest under pressure after electrodeposition. SEM images in Figure S10 highlight a smoother and denser morphology of Na deposits involving a 2h rest.

Finally, 100 plating/stripping cycles using 30 min plating time at 5 mA cm⁻² were conducted without rest or with a 2 hour rest between cycles (Figures 5F, 5G). Without rest, the voltage profiles exhibit soft-short behavior likely due to dendrite or 3-D Na formation at these high currents, but the devices exposed to 2h rest at the same rate after electroplating showed a stable response with CE% after 100 cycles of 99.7% (Figure S11). These findings indicate the electrochemical stability of Na metal deposits at pressure conditions of standard coin and pouch cell packaging is dependent upon the interplay between morphological evolution and creep of the electrodeposited sodium metal and the rate at which the sodium metal is electrodeposited (i.e. the current density) used in experiments. Building from our findings, this interplay is visualized in Figure 5H, where under conditions of low morphological evolution or creep, such as at low pressures, the Na deposits exhibit 3-D architectures and dendrite formation. However, at higher pressures > 500 kPa, the influence of creep and/or morphological evolution of the sodium leads to smooth layers with stable and efficient electrochemical behavior. Notably, such higher pressure conditions can still lead to 3-D morphologies and shorting effects if the current density is too high (e.g. faster than the rate of sodium evolution on the current collector surface), but as our results showed in Figure 5, this effect can be reversed by rest periods which facilitate the evolution toward a smooth sodium deposit.

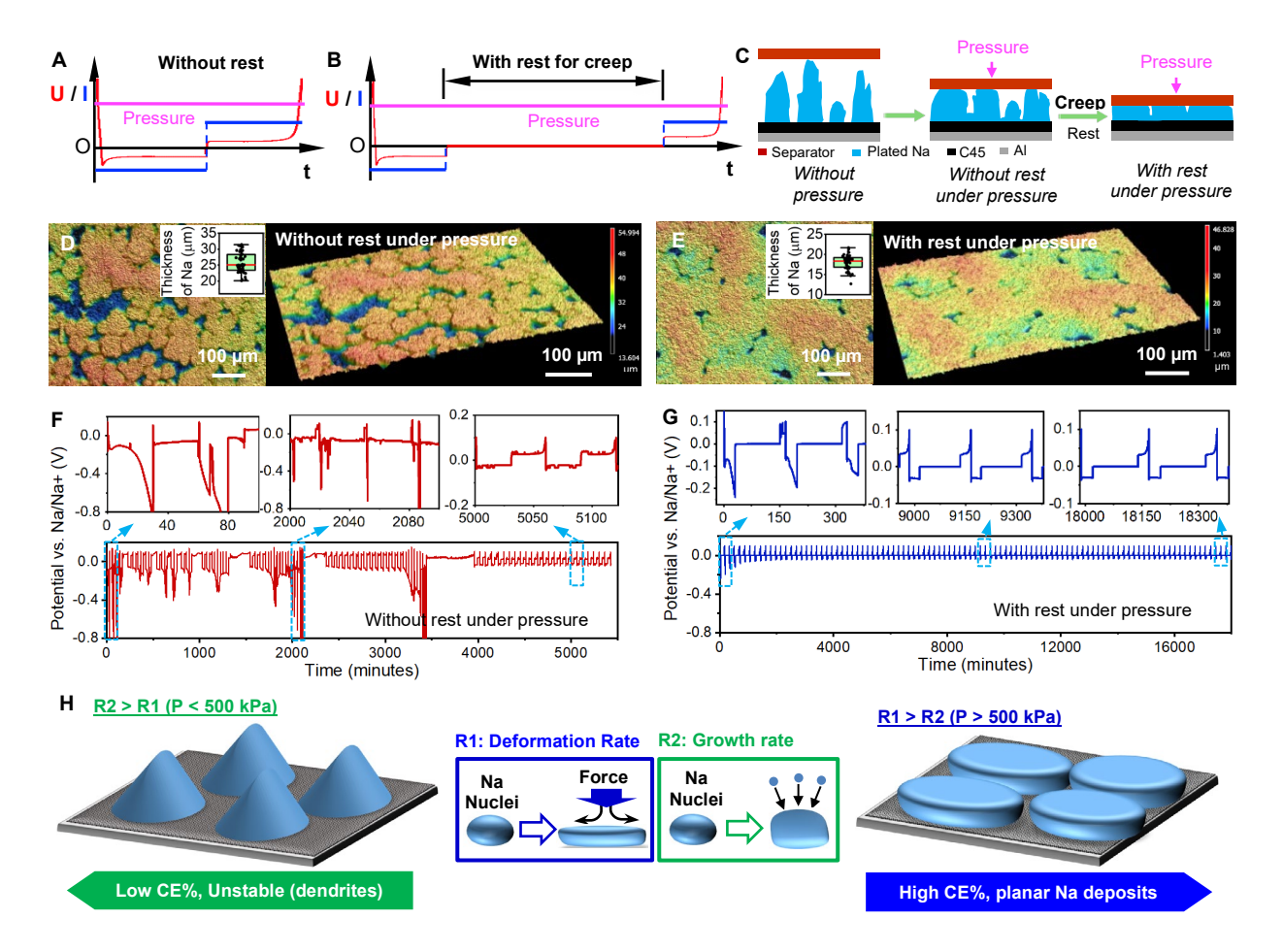


Figure 5. The effect of pressure-driven creep on Na deposits. Schematic of plating/stripping test regime for (A) without rest, and (B) with a 2 hour rest between each plating and stripping step, note that the plating current density and time is 5 mA cm⁻² and 0.5 h, respectively. (C) Schematic illustration of pressure-driven creep effect on Na deposits. CSLM images of Na deposits (D) without rest, and (E) with rest under pressure, as well as the corresponding thickness of Na deposits obtained from CSLM test (inset). Cycling performance at 5 mA cm⁻² (F) without rest, and (G) with 2 hour rest under pressure in coin cells with enlarged voltage profiles. (H) Schematic of the interplay between the sodium deposition rate and the rate of mechanical deformation and morphology evolution of sodium metal deposits as we observe in this study.

In summary, our findings give insight into the coupled chemo-mechanical behavior that is responsible for the stable, high-performance of sodium metal batteries widely reported in the literature. Our results indicate that dynamic creep and morphology evolution of electrodeposited sodium at pressures relevant to coin and pouch cell packaging (500 kPa to 1.2 MPa) are responsible for the smooth sodium deposits that are correlated to high CE%, which over many cycles can exceed 99.9% consistent with our observations in this work. Unlike Li metal deposits, which are mostly static at pressures of 500 kPa – 1.2 MPa, our results suggest that a key factor in stable Na metal deposits is the dynamic mechanical behavior of Na in this pressure range. We hypothesize from this work that mechanics and corresponding transport behavior of electrodeposited Na on different current collector materials could be equally important, if not more important, than controlled nucleation behavior for sodium metal batteries.

ASSOCIATED CONTENT

Supporting Information

Detailed experiment methods, SEM image, supplementary plating/stripping voltage files, schematics of pressure cell, coin cell, and airtight optical cell, plot of CE versus cycle number for high current devices with and without rest periods (PDF)

AUTHOR INFORMATION

Corresponding Author

Cary L. Pint – Department of Mechanical Engineering, Iowa State University, Ames, Iowa 50011, United States; Email: carypint@iastate.edu

Authors

Weimin Jiao – Department of Mechanical Engineering, Iowa State University, Ames, Iowa 50011, United States

Murtaza Zohair – Department of Mechanical Engineering, Iowa State University, Ames, Iowa 50011, United States

Janna Eaves-Rathert – Department of Mechanical Engi-neering, Vanderbilt University, Nashville, Tennessee 37235, United States

Jayanth Ramaswami Ramamurthy – Department of Mechanical Engineering, Iowa State University, Ames, Iowa 50011, United States

Rebecca Mort – Department of Materials Science and Engineering, Iowa State University, Ames, Iowa 50011, United States

Jacob Wheaton – Department of Materials Science and Engineering, Iowa State University, Ames, Iowa 50011, United States

Shan Jiang – Department of Materials Science and Engineering, Iowa State University, Ames, Iowa 50011, United States

Steve W. Martin – Department of Materials Science and Engineering, Iowa State University, Ames, Iowa 50011, United States

Notes

The authors declare no competing financial interest.

ACKNOWLEDGMENT

(Word Style "TD_Acknowledgments"). Generally the last paragraph of the paper is the place to acknowledge people, organizations, and financing (you may state grant numbers and sponsors here). Follow the journal's guidelines on what to include in the Acknowledgments section.

Partial support of this work by SWM was provided by the NSF through grant DMR 1936913 and by the State of Iowa through grant IEC/IED 307352.

REFERENCES

- (1) Seh, Z. W.; Sun, J.; Sun, Y.; Cui, Y., A Highly Reversible Room-Temperature Sodium Metal Anode. *ACS Cent. Sci.* **2015**, *1*, 449-455.
- (2) Sun, B.; Xiong, P.; Maitra, U.; Langsdorf, D.; Yan, K.; Wang, C.; Janek, J.; Schröder, D.; Wang, G., Design Strategies to Enable the Efficient Use of Sodium Metal Anodes in High-Energy Batteries. Adv. Mater. 2020, 32, 1903891.
- (3) Zhao, Y.; Adair, K. R.; Sun, X., Recent developments and insights into the understanding of Na metal anodes for Na-metal batteries. *Energy Environ. Sci.* **2018**, *11*, 2673-2695.
- (4) Cohn, A. P.; Muralidharan, N.; Carter, R.; Share, K.; Pint, C. L., Anode-Free Sodium Battery through in Situ Plating of Sodium Metal. *Nano Lett.* **2017**, *17*, 1296-1301.
- (5) Li, Y.; Zhou, Q.; Weng, S.; Ding, F.; Qi, X.; Lu, J.; Li, Y.; Zhang, X.; Rong, X.; Lu, Y.; Wang, X.; Xiao, R.; Li, H.; Huang, X.; Chen, L.; Hu, Y.-S., Interfacial engineering to achieve an energy density of over 200 Wh kg-1 in sodium batteries.

 Nat. Energy 2022, 7, 511-519.

- (6) Hartmann, P.; Bender, C. L.; Vračar, M.; Dürr, A. K.; Garsuch, A.; Janek, J.; Adelhelm, P., A rechargeable room-temperature sodium superoxide (NaO2) battery. *Nat. Mater.* **2013**, *12*, 228-232.
- (7) Reeve, Z. E. M.; Franko, C. J.; Harris, K. J.; Yadegari, H.; Sun, X.; Goward, G. R., Detection of Electrochemical Reaction Products from the Sodium–Oxygen Cell with Solid-State 23Na NMR Spectroscopy. *J. Am. Chem. Soc.* **2017**, *139*, 595-598.
- (8) Xia, C.; Fernandes, R.; Cho, F. H.; Sudhakar, N.; Buonacorsi, B.; Walker, S.; Xu, M.; Baugh, J.; Nazar, L. F., Direct Evidence of Solution-Mediated Superoxide Transport and Organic Radical Formation in Sodium-Oxygen Batteries. J. Am. Chem. Soc. 2016, 138, 11219-11226.
- (9) Wang, Y.-X.; Yang, J.; Lai, W.; Chou, S.-L.; Gu, Q.-F.; Liu, H. K.; Zhao, D.; Dou, S. X., Achieving High-Performance Room-Temperature Sodium-Sulfur Batteries With S@Interconnected Mesoporous Carbon Hollow Nanospheres. *J. Am. Chem. Soc.* 2016, 138, 16576-16579.
- (10) Wei, S.; Xu, S.; Agrawral, A.; Choudhury, S.; Lu, Y.; Tu, Z.; Ma, L.; Archer, L. A., A stable room-temperature sodium–sulfur battery. *Nat. Commun.* **2016,** *7*, 11722.
- (11) Xin, S.; Yin, Y.-X.; Guo, Y.-G.; Wan, L.-J., A High-Energy Room-Temperature Sodium-Sulfur Battery. *Adv. Mater.* **2014**, *26*, 1261-1265.

- (12) Wang, H.; Matios, E.; Luo, J.; Li, W., Combining theories and experiments to understand the sodium nucleation behavior towards safe sodium metal batteries. *Chem. Soc. Rev.* **2020**, *49*, 3783-3805.
- (13) Lee, B.; Paek, E.; Mitlin, D.; Lee, S. W., Sodium Metal Anodes: Emerging Solutions to Dendrite Growth. *Chem. Rev.* **2019**, *119*, 5416-5460.
- (14) Peters, J.; Buchholz, D.; Passerini, S.; Weil, M., Life cycle assessment of sodiumion batteries. *Energy Environ. Sci.* **2016**, *9*, 1744-1751.
- (15) Yui, Y.; Hayashi, M.; Nakamura, J., In situ Microscopic Observation of Sodium Deposition/Dissolution on Sodium Electrode. *Sci. Rep.* **2016**, *6*, 22406.
- (16) Ma, B.; Lee, Y.; Bai, P., Dynamic Interfacial Stability Confirmed by Microscopic Optical Operando Experiments Enables High-Retention-Rate Anode-Free Na Metal Full Cells. *Adv. Sci* **2021**, *8*, 2005006.
- (17) Cohn, A. P.; Metke, T.; Donohue, J.; Muralidharan, N.; Share, K.; Pint, Cary L., Rethinking sodium-ion anodes as nucleation layers for anode-free batteries. *J. Mater. Chem. A* **2018**, *6*, 23875-23884.

- (18) Masias, A.; Felten, N.; Garcia-Mendez, R.; Wolfenstine, J.; Sakamoto, J., Elastic, plastic, and creep mechanical properties of lithium metal. *J. Mater. Sci.* **2019**, *54*, 2585-2600.
- (19) Wang, M. J.; Chang, J.-Y.; Wolfenstine, J. B.; Sakamoto, J., Analysis of elastic, plastic, and creep properties of sodium metal and implications for solid-state batteries. *Materialia* **2020**, *12*, 100792.
- (20) Fincher, C. D.; Zhang, Y.; Pharr, G. M.; Pharr, M., Elastic and Plastic Characteristics of Sodium Metal. *ACS Appl. Energy Mater.* **2020,** *3*, 1759-1767.
- (21) Yin, X.; Tang, W.; Jung, I. D.; Phua, K. C.; Adams, S.; Lee, S. W.; Zheng, G. W., Insights into morphological evolution and cycling behaviour of lithium metal anode under mechanical pressure. *Nano Energy* **2018**, *50*, 659-664.
- (22) Shen, X.; Zhang, R.; Shi, P.; Chen, X.; Zhang, Q., How Does External Pressure Shape Li Dendrites in Li Metal Batteries? *Adv. Energy Mater.* **2021,** *11*, 2003416.
- (23) Zhang, X.; Wang, Q. J.; Peng, B.; Wu, Y., Pressure-Driven and Creep-Enabled Interface Evolution in Sodium Metal Batteries. *ACS Appl. Mater. Interfaces* **2021**, *13*, 26533-26541.

- (24) Spencer Jolly, D.; Ning, Z.; Darnbrough, J. E.; Kasemchainan, J.; Hartley, G. O.; Adamson, P.; Armstrong, D. E. J.; Marrow, J.; Bruce, P. G., Sodium/Na β " Alumina Interface: Effect of Pressure on Voids. *ACS Appl. Mater. Interfaces* **2020**, *12*, 678-685.
- (25) Harrison, K. L.; Goriparti, S.; Merrill, L. C.; Long, D. M.; Warren, B.; Roberts, S. A.; Perdue, B. R.; Casias, Z.; Cuillier, P.; Boyce, B. L.; Jungjohann, K. L., Effects of Applied Interfacial Pressure on Li-Metal Cycling Performance and Morphology in 4 M LiFSI in DME. ACS Appl. Mater. Interfaces 2021, 13, 31668-31679.
- (26) Qin, L.; Wang, K.; Xu, H.; Zhou, M.; Yu, G.; Liu, C.; Sun, Z.; Chen, J., The role of mechanical pressure on dendritic surface toward stable lithium metal anode. *Nano Energy* **2020**, *77*, 105098.
- (27) Schneider, C. A.; Rasband, W. S.; Eliceiri, K. W., NIH Image to ImageJ: 25 years of image analysis. *Nat. Meth.* **2012**, *9*, 671-675.
- (28) Zhang, X.; Wang, Q. J.; Harrison, K. L.; Roberts, S. A.; Harris, S. J., Pressure-Driven Interface Evolution in Solid-State Lithium Metal Batteries. *Cell Rep. Phys. Sci.* **2020**, *1*, 100012.